Tropoelastin coated tendon biomimetic scaffolds promote stem cell tenogenic commitment and deposition of elastin-rich matrix

Helena Almeida,[1,2] Rui M. A. Domingues,[1,2,3] Suzanne M. Mithieux,[4,5] Ricardo A. Pires,[1,2,3] Ana I. Gonçalves,[1,2] Manuel Gómez-Florit,[1,2] Rui L. Reis,[1,2,3], Anthony S. Weiss,[4,5,6] and Manuela E. Gomes[1,2,3*]*

[1]3B's Research Group, I3Bs – Research Institute on Biomaterials, Biodegradables and Biomimetics, University of Minho, Headquarters of the European Institute of Excellence on Tissue Engineering and Regenerative Medicine, AvePark, Parque de Ciência e Tecnologia, Zona Industrial da Gandra, 4805-017 Barco, Guimarães, Portugal;

[2]ICVS/3B's–PT Government Associate Laboratory, Braga/Guimarães, Portugal;

[3]The Discoveries Centre for Regenerative and Precision Medicine, Headquarters at University of Minho, Avepark, 4805-017 Barco, Guimarães, Portugal.

[4] School of Life and Environmental Sciences, University of Sydney, NSW 2006, Australia;

[5]Charles Perkins Centre, University of Sydney, NSW 2006, Australia;

[6]Bosch Institute, University of Sydney, NSW 2006, Australia.

KEYWORDS

Biomimetic, hierarchical scaffolds, tropoelastin, polydopamine, human-adipose derived stem cells, tenogenic differentiation, elastin *de novo* synthesis

ABSTRACT

Tendon tissue engineering strategies that recreate the biophysical and biochemical native microenvironment have a greater potential to achieve regeneration. Here, we developed tendon biomimetic scaffolds using mechanically competent yarns of poly-ε-caprolactone, chitosan and cellulose nanocrystals to recreate the inherent tendon hierarchy from the nano to macro scale. These were then coated with tropoelastin (TROPO) through polydopamine linking (PDA), to mimic the native extracellular matrix (ECM) composition and elasticity. Both PDA and TROPO coatings decreased surface stiffness without masking the underlying substrate. We found that human adipose-derived stem cells (hASCs) seeded onto these TROPO biomimetic scaffolds more rapidly acquired their spindle-shape morphology and high aspect ratio characteristic of tenocytes. Immunocytochemistry shows that the PDA and TROPO-coated surfaces boosted

differentiation of hASCs towards the tenogenic lineage, with sustained expression of the tendon-related markers scleraxis and tenomodulin up to 21 days of culture. Furthermore, these surfaces enabled the deposition of a tendon-like ECM, supported by the expression of collagens type I and III, tenascin and decorin. Gene expression analysis revealed a downregulation of osteogenic and fibrosis markers in the presence of TROPO when compared with the control groups, suggesting proper ECM deposition. Remarkably, differentiated cells exposed to TROPO acquired an elastogenic profile due to the evident elastin synthesis and deposition, contributing to the formation of a more mimetic matrix in comparison with the PDA-coated and uncoated conditions. In summary, our biomimetic substrates combining biophysical and biological cues modulate stem cell behavior potentiating their long-term tenogenic commitment and the production of an elastin-rich ECM.

INTRODUCTION

Tendons injuries are often painful and debilitating, and are particularly common among elderly, athletic and actively working populations. In addition to their extremely low and inefficient natural healing capacity due to the hypovascular and hypocellular nature, injured tendons respond poorly to standard treatments as the native strength and functionality of tissue prior to injury does not fully recover.[1–3] Tissue engineering has

contributed alternative strategies for tendon repair and regeneration, with the most promising ones being those that mimic the composition and structure of the native tissue, along with suitable mechanical properties.

In tendons, organization starts at the molecular level with three collagen type I molecules crosslinking as triple helices and further assembling into collagen fibrils at approximately 100 nm diameter. Fibrils assemble into fibers longitudinally aligned to the tendon long axis, at 1 to 20 μm diameter. These structures along with scarce spindle-shaped cells, the tenocytes, form the fascicles.[1,3] In addition to type I collagen, which represents 60% of the total tendon dry mass, the hydrated extracellular matrix (ECM) also comprises up to 4% elastin, located in elastic fibers that are parallelly interspersed within the tissue.[4–6] Elastin is an extremely durable protein responsible for handling the repetitive and reversible elastic recoil of tendons, and whose turnover is limited due to reduced postnatal elastogenesis.[7]

The fibrillar and aligned architecture of the tendon niche *in vivo* has been recapitulated in scaffolds, demonstrating the reprogramming capacity of nanotopographic cues on stem cells phenotype and fate. In general, nanofibrous and anisotropic topographies are prone to induce regenerative responses by cells.[8,9] Moreover, these same features have been combined and applied to hierarchic constructs, where they are able to drive stem cell tenogenic differentiation and/or avoid the phenotypic drift of tenocytes.[10,11]

Nonetheless, the way cells modulate their morphology and orientation reflects their interactions with the substrate, not only by means of topography, but also through surface chemistry and elasticity.[12,13] Hence, strategies combining both biophysical and biological/biochemical cues are likely to induce a more adequate response towards neotissue formation when the tendon niche is closely mimicked. The incorporation of ECM proteins in regenerative templates to emulate the natural cell environment is an interesting way to guide cells responses.[14] Pang *et al*.[15] recently studied the relationship between tenocytes and fibrillar components of the native ECM, including collagen and elastin. They show that elastin forms a thin mesh-layer around tenocytes within the longitudinal collagen fibril network suggesting a crosstalk between these elements.[15]

Therefore, elastin holds unexplored potential in the tendon tissue engineering field. However its crosslinked and insoluble nature makes its processing challenging.[16] Tropoelastin (TROPO), on the other hand, is the soluble precursor of elastin and has been used to effect in diverse applications.[17] Recombinant human TROPO promotes elastin *de novo* synthesis when used as a medium supplement in elastogenic cell culture.[7,18–20] In a tissue engineering perspective, TROPO has been incorporated as a bulk material to build highly elastic hydrogels,[21,22] films produced through casting[23] or electrospun fibrous scaffolds[24,25] to enhance cell adhesion, proliferation and migration, neo-vascularization and even direct stem cell commitment.[26] TROPO has also been covalently bounded to

plasma activated surfaces to enhance cell attachment and potentiate integration within the body.[27,28]

Based on the potential role of elastin over native tenocytes, here we propose a novel biomimetic strategy that combines the advantages of 3D nano-to-macro hierarchical and anisotropic scaffolds with the biological potential of TROPO. Our hypothesis is that coating such scaffolds with TROPO will result in bioactive biomaterials that mimic the biophysical and biochemical microenvironment, fostering stem cell differentiation towards the tenogenic lineage and enhancing the deposition of a tendon-like matrix rich in elastin. For this, and building on our previous tendon mimetic fibrous system,[11] we produced yarns made of continuous and aligned electrospun nanofibrous threads (CANT) based on a poly-ε-caprolactone (PCL)/chitosan (CHT) polymer blend mechanically reinforced with cellulose nanocrystals (CNCs), which were coated with TROPO and used as representative units (fascicles) of tendons.

MATERIALS AND METHODS

Materials. Poly-ε-caprolactone (PCL, average Mn 80,000), chitosan medium molecular weight (CHT), microcrystalline cellulose (MCC, Avicel PH-101), dopamine hydrochloride, phosphate buffered saline (PBS), bovine serum albumin (BSA), phalloidin tetramethylrhodamine B isothiocyanate (phalloidin) and collagenase type I A were purchased from Sigma-Aldrich. Acetic acid glacial (AA), Triton X-100 and neutral

buffered formalin 10% (v/v) were acquired from Thermo Fisher Scientific. Ribozol was obtained from Amresco, sulfuric acid 96% from Carlo Erba, formic acid (FA) from Panreac AppliChem, tris base and sodium dodecyl sulfate (SDS) from NZYTech, 4,6–diamidino-2-phenyindole dilactate (DAPI) from Biotium and normal horse serum 2.5% from Vector Laboratories. Minimum essential medium alpha (α-MEM), antibiotic/antimycotic solution (AB/AM), fetal bovine serum (FBS) and TrypLE Express with phenol red were purchased from Life Technologies. Antibody diluent with background reducing components was obtained from Dako, Alexafluor 488 donkey anti-rabbit and anti-mouse were from Invitrogen. The rabbit polyclonal anti-C-terminal tenomodulin antibody against a synthetic polypeptide compliant to amino acids 245-252 of mouse and human, was kindly produced and provided by Prof. Denitsa Docheva.[29]

Production of biomimetic yarns. The CANT made of PCL/CHT/CNCs were produced by electrospinning and assembled into yarns as described previously.[11,30] First, CNCs were isolated from MCC powder through sulfuric acid hydrolysis and characterized using atomic force microscopy (AFM) (see Supporting Information), and CHT was purified by dissolution in an acetic acid solution followed by a series of filtration and precipitation steps (see Supporting Information). Briefly, spray-dried CNCs (3% w/w, relative to the polymeric blend matrix (PCL/CHT)) were first dispersed in formic acid. Then PCL (11% w/w, relative to solvent mass) was dissolved in the suspension for 2.5 h, and afterwards glacial acetic acid was added to make a 7:3 FA/AA volume ratio and the

solution was left to stir, until complete dissolution of the PCL. Meanwhile, CHT was dissolved (4% w/w) in a solvent mixture of FA/AA (7:3, v/v), with stirring for 3 h at 70°C. The final solution of PCL/CHT/CNC was prepared by mixing solution 1 (11% w/w PCL and CNCs contents representing 3% w/w of the final polymer blend matrix, in AA/FA) with solution 2 (4% w/w CHT in AA/FA) at a 7:3 ratio, respectively. The CANT were produced with a customized electrospinning device based on the setup proposed by Khil *et al*.[31] The polymer/CNC solution contained in a syringe (12.25 mm diameter) with a fitted 21G needle was electrospun at a constant flow rate of 0.45 $mL.h^{-1}$ and an applied voltage of 22-24 kV. A vertical distance of 14 cm from the tip of the needle to the surface of the grounded water/ethanol (8:2, v/v) support liquid bath and a horizontal distance of 20 cm from the tip of the needle to the collecting roller were set. CANT were collected at a constant speed of 0.01 $m.s^{-1}$ and tendon mimetic scaffolds assembled by grouping 12 threads together and twisting 4 $turns.cm^{-1}$ to form yarns. Threads were collected at room temperature (22 ± 2 °C) with the humidity varying from 40 to 50%.

Surface functionalization of yarns with TROPO. The yarns previously prepared were cut into 2 cm length pieces and coated with PDA, as suggested by Lee *et al*.[32] with slight modifications. Briefly, yarns were placed inside an open vessel with 10 mM Tris buffer at pH 8.5 and dopamine hydrochloride was added to achieve a 1 $mg.mL^{-1}$ solution, initiating the spontaneous reaction of PDA self-polymerization. Mild shaking was applied to avoid non-specific microparticle deposition at the surface of the yarns and

ensure an even oxygen distribution. The coating was carried for 8 h, after which samples were collected and rinsed thoroughly with distilled water to remove unadhered PDA particles. Recombinant mature wild-type human TROPO without domain 26A (isoform SHELΔ26A), corresponding to residues 27 to 724 of GenBank entry AAC98394 was produced and purified from bacteria on a multi-gram scale, in the Weiss lab (Sydney, Australia) as described elsewhere.[33] For TROPO conjugation, PDA-coated yarns were dipped in a 20 $\mu g.mL^{-1}$ TROPO in 10 mM Tris buffer at pH 8.5, overnight (12-16h) at 4 °C and under gentle shaking. After the coating, samples were rinsed with PBS to remove excess unbound protein and used immediately or left to dry for further characterization.

Physical characterization of the functionalized yarns. The morphology and the topography of the uncoated, PDA-coated and TROPO/PDA-coated yarns were assessed by high-resolution scanning electron microscopy (SEM, Auriga CompactLV from Zeiss), operating at an accelerating voltage of 5 kV. Prior to imaging, the samples were sputter-coated with ~4 nm platinum (Cressington). The diameters of the yarns and nanofibers (at least 100 randomly selected) were determined from several micrographs using ImageJ software (version: 1.50b, NIH, USA). Surface roughness and architecture were also evaluated using AFM Dimension Icon (Bruker, USA). The scans were collected in PeakForce QNM in air mode with a MultiMode atomic force microscope (AFM) connected to a NanoScope V controller (Veeco, USA). AFM cantilevers (RTESPA-150, Bruker) made of silicon were used, with spring constants of 6 $N.m^{-1}$ and frequency of 150

kHz. Several micrographs were collected, and these were then analyzed with the Gwyddion software (version: 2.43) to determine the root-mean-square roughness of the surfaces and generate the 3D projections. The nanomechanical properties of the uncoated, PDA-coated and TROPO/PDA-coated surfaces were analyzed with an AFM (NanoWizard 3, JPK Instruments, Germany), using ACST probes (typical k~7.8N.m^{-1}, AppNano, USA) under Force Mapping mode. Before analysis, the probe was calibrated under PBS using the contact-based method and the sensitivity and k were determined. For the AFM analysis, each sample was mounted under a hydrated medium (PBS, at 37°C) and 8x8 maps were recorded using square acquisition frames of 10x10μm. Individual force curves were collected using a z length of 20μm and a relative setpoint of 7.5 nN. The Young's modulus of each analyzed sample position was calculated from the corresponding force curve by fitting the Hertz/Sneddon model using the JPK SPM Data Processing software (JPK Instruments) and using a Poisson ratio fixed at 0.5. For all the samples, at least 3 force maps were collected at different sample positions.

Surface characterization of the functionalized yarns. The success of the PDA coating was assessed with spectroscopic techniques, namely Fourier transform infrared spectroscopy in attenuated total reflectance mode (FTIR-ATR) and Raman spectroscopy (see Supporting Information). For TROPO detection, FTIR-ATR spectra of uncoated yarns, uncoated yarns dipped in TROPO without PDA, PDA-coated and TROPO/PDA-coated yarns, as well as TROPO alone were first collected as described in detail in

Supporting Information. Afterwards, spectra of samples without TROPO were subtracted from the corresponding spectra of the TROPO-coated samples, thus obtaining the infrared signal exclusively from the elastin precursor. For all the previous tests, at least 5 different areas from each sample were analyzed, using 3 replicates per condition. Moreover, the extent of covalent binding of TROPO to the surface of the yarns was determined through antibody detection (see Supporting Information).

Cell seeding. Human adipose tissue-derived stem cells (hASCs) were isolated from lipoaspirate samples obtained from donors that signed an informed consent according to the Declaration of Helsinki. All the procedures were approved by the Ethical Committee of University of Minho. The hASCs isolation and stemness characterization were performed following a protocol described elsewhere.[34] Briefly, the tissue samples were thoroughly washed with PBS and digested with 0.05% collagenase Type I A in PBS for 60 min at 37 ºC under gentle stirring. Then, cells were centrifuged and the cell pellet was resuspended in complete cell culture medium (α-MEM supplemented with 10% (v/v) FBS and 1% (v/v) AB/AM) and seeded in culture flasks. After 24h of incubation under standard cell culturing conditions, the adherent cells were washed and their stemness was evaluated through flow cytometry for the expression of mesenchymal stem cell markers (CD45, CD105 and CD90), as shown previously.[35] For all experiments, hASCs were used at passage 3-5. Uncoated yarns were cut into ~2 cm pieces and vacuum dried overnight in a desiccator, to eliminate possible solvent and/or water/ethanol residues

remaining from the production process. These were then sterilized by immersion in 70% (v/v) ethanol for 1 h, followed by two washes with sterile DPBS (15 min each). The yarns were then divided by conditions, with both the PDA- and the TROPO/PDA-coatings being kept under sterile conditions inside a laminar flow cabinet, and with solutions being filtered prior to the coatings. Afterwards, samples were mounted onto sterile inserts (CellCrown-24, Scaffdex, Finland) exposing 1.3 cm length of the yarns, which were then placed in 24-well low adhesion culture plates and rinsed with sterile DPBS. Samples were pre-incubated for ~3 h in complete cell culture medium, at 37 °C and 5% CO_2, to further promote cell adhesion. Meanwhile, hASCs were trypsinized and seeded onto the yarns at a density of 1×10^5 cells per well, using 1 mL of cell suspension in complete cell culture medium, under standard culturing conditions. The medium was changed twice a week over the course of the different biological assays.

Cell morphology evaluation. Cell morphology and organization were assessed through confocal microscopy, by staining cell nuclei and cytoskeleton actin filaments with DAPI and phalloidin, respectively. Samples cultured for 5 days were fixed with neutral buffered formalin 10% (v/v) for 20 min at room temperature, after being washed twice with PBS. Following two other washings, samples were removed from the inserts and cells permeabilized with 0.1% (v/v) Triton X-100 in PBS for 10 min, at room temperature under mild agitation. To this step two washes in PBS followed, each taking 5 min. A solution of DAPI (1:1000, v/v) and phalloidin (1:200, v/v) was prepared in PBS,

and each sample was incubated for 30 min at room temperature, with mild agitation and protected from light. Samples were rinsed with PBS to eliminate excess dye, mounted on microscopic sample holders and observed through confocal laser scanning microscopy (Leica TCS SP8, Microsystems, Wetzlar, Germany). Several representative micrographs were collected from four samples per condition. The nuclear aspect ratio of hASCs was determined by measuring the length and width of at least 50 nuclei for each condition. The measurements were performed using ImageJ software on several micrographs. The nuclei aspect ratio (AR) was determined by dividing the length by the width of the nuclei, which denotes elongation when higher than 1.

Cell proliferation assessment. The proliferation of hASCs was determined through DNA quantification of cell lysates, using the Quant-iT™ PicoGreen® dsDNA kit (Life Technologies), for days 5 and 14 of cell culture.

Immunofluorescence staining for tendon-related markers. Before staining, yarns seeded with cells were washed twice with PBS and the cells were then fixed and permeabilized. All samples were blocked with normal horse serum 2.5% for 40 min at room temperature, to avoid non-specific reactions. The serum was gently removed and the immunostaining was performed using primary antibodies against scleraxis (rabbit anti-SCXA-aminoterminal end antibody, Abcam, ab58655, 1:200), tenomodulin (rabbit anti-tenomodulin antibody, 1:200) and tenascin (mouse anti-tenascin-C antibody, MA1-26779, Thermo Fisher Scientific, 1:3000), and samples incubated overnight, at 4 °C.

Alternatively, samples were incubated with either BA4 mouse anti-elastin antibody (E4013, Sigma-Aldrich, 1:500) or rabbit anti-collagen type I antibody (ab90395, Abcam, 1:500) for 1.5 hours at room temperature. Afterwards, all samples were incubated with hydrogen peroxide (0.3%, v/v) for 15 min and then incubated with the respective fluorescent-labeled secondary antibody (AlexaFluor 488 donkey anti-rabbit, A21206, 1:200 or AlexaFluor 488 donkey anti-mouse, A21202, 1:200) at room temperature for 1 h, protected from light. All antibodies were diluted in antibody diluent with background reducing components. Finally, samples were once again rinsed with PBS, and cell cytoskeleton and nuclei were counterstained with phalloidin (1:200 in PBS) and DAPI (1:1000 in PBS) respectively, at room temperature for 30 min. After washing, the samples were kept in PBS at 4 °C until further use. Immunolabeled samples were analyzed through confocal laser scanning microscopy. For samples stained for scleraxis, tenomodulin, tenascin and collagen type I, a minimum of 3 Z-stacks from different fields of view were converted to maximum projections to determine the yarn area stained with each antibody, which was further divided by the area stained with DAPI corresponding to cell nuclei. A threshold was applied to each channel to discard background pixels and then the area of green pixels was divided by the area of blue pixels. For elastin-labeled samples a minimum of 4 Z-stacks from different fields of view were converted to maximum projections to determine the percentage of yarn area stained with the anti-elastin antibody. The same threshold was applied to all images to discard background

pixels and then the area of green pixels measured and converted to a percentage per total yarn area.

Ribonucleic acid extraction and real-time polymerase chain reaction. The influence of the substrate on the tenogenic differentiation of hASCs and ECM remodeling was evaluated after 14 days of culture through real-time polymerase chain reaction (qPCR) analysis. Total ribonucleic acid (RNA) was isolated with Ribozol and quantified using the Nanodrop spectrophotometer (ThermoFisher Scientific, USA) at 260 nm. Then, solutions of 15 μL with 1 μg of RNA were prepared, by diluting RNA samples in RNAse/DNAse free water. Complementary DNA (cDNA) was synthesized through reverse transcription of RNA following the supplier instructions using the qScript cDNA Synthesis Kit (Quanta Biosciences, USA). The cDNA was diluted in RNAse/DNAse free water and samples kept in the -20 °C until further use. qPCR was carried out to assess the expression of the markers presented in Table S1 (see Supporting Information) using as reference genes glyceraldehyde-3-phosphate dehydrogenase (*GAPDH*) and beta-actin (*ACTB*), through SYBR green detection. In each well, 7 μL of a master mix solution (Perfecta SYBR Green FastMix, Quanta Biosciences, USA) containing the reverse and forward primers (0.5 μM), was mixed with 3 μL of each cDNA sample, to a final volume of 10 μL. Amplification of the genes was performed in a thermocycler (Realplex, Eppendorf, Germany), initiated with the pre-incubation step for denaturation of the cDNA template (5 min, 95 °C), followed by the denaturation step including 45 cycles (10 sec, 95 °C), the annealing step

(10 sec, 60 °C) and finally the extension step (10 sec, 72 °C). At the end of each cycle, fluorescence was measured at 72 °C. Blanks were considered for each primer as a negative control. Samples were normalized by the geometric mean of the expression levels of the reference genes and the mRNA expression levels were calculated according to the ΔΔCt method relative to the uncoated samples or, if expression was not detected for this group, relative to the PDA samples.

Stiffness evaluation of the deposited matrices. The nanomechanical properties of the ECM deposited on the surface of uncoated, PDA-coated and TROPO/PDA-coated samples after 21 days of culture were analyzed using an atomic force microscope (JPK NanoWizard 3, JPK Instruments, Germany) using qp-BioAC-CB2 probes (typical $k \sim 0.1 N.m^{-1}$, Nanosensors, Switzerland) under Force Mapping mode using the same conditions as described for the cell-free samples. Cantilevers were calibrated using the contact-based method prior analysis. Samples were mounted under cell culture medium at 37 °C. The same procedure, as previously described for the cell-free samples, was used to determine the Young's modulus of each sample. At least 3 force maps were collected at different sample positions.

Statistical analysis. Results are presented as mean values ± SD (standard deviation). The statistical analysis of data was performed using GraphPad PRISM version 7.0. After testing for normality, one-way analysis of variance (ANOVA) followed by the Tukey post hoc test for multiple comparisons or a Kruskal–Wallis test followed by Dunn's test were

performed to compare groups of variables. Statistical significance was set to $p < 0.05$, represented by symbols described in the graphs.

RESULTS AND DISCUSSION

Surface functionalization and characterization of tendon hierarchical scaffolds. CANT were produced by electrospinning a blend of PCL and CHT mechanically reinforced with CNCs.[30] Then, yarns of 12 threads were manually assembled (Figure 1A), to obtain tendon nanocomposite hierarchical scaffolds that recreate the collagen fiber fascicles architecture seen in native tissues, which were used as a substrate for this work. In addition, the yarns can be further assembled into 3D scaffolds to recapitulate the fibrous nano-to-macro hierarchical structure and the mechanical behavior of native tendon (tensile Young's Modulus of ~200 MPa and ultimate tensile strength of ~40 MPa).[11] The functionalization of anisotropic yarns surface with TROPO was performed via PDA mediated linkage in two consecutive and straightforward dip-coating steps (Figure 1B). Bioinspired by the adhesive properties of the *Mytilus edulis* foot protein 5 found in marine mussels,[36] PDA has been widely used in tissue engineering strategies as a simple, versatile and biocompatible linker to functionalize different biomaterial surfaces without negatively impacting their bulk mechanical properties,[37] an important requisite in the context of engineered tendon scaffolds.

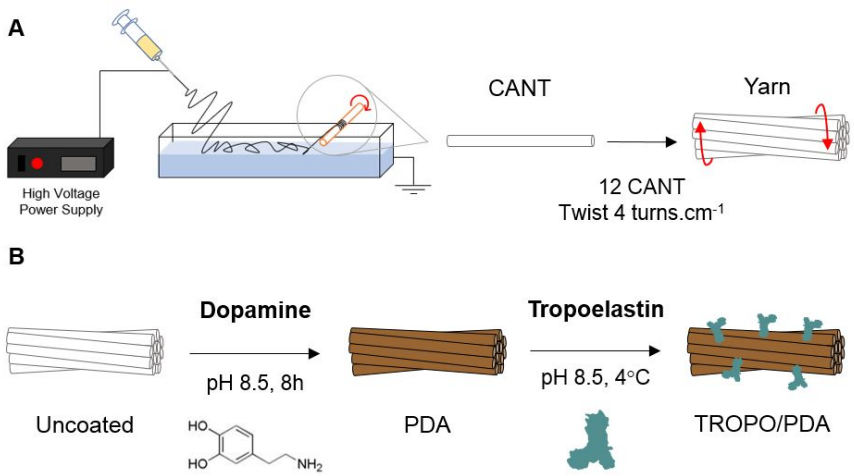

Figure 1. Schematic representation of general strategy to obtain functional biomimetic tendon scaffolds. A) Electrospinning setup for CANT production and assembly into yarns of 12 threads mimicking tendon collagen fascicles; and B) Immobilization of TROPO on the surfaces of yarns via PDA linking.

Physical and chemical characterization of the coatings. The surface morphology and roughness of yarns were evaluated by SEM and AFM to ensure that the nanofibrous architecture and topography of the starting yarns was not masked by the PDA and TROPO coatings. SEM images revealed that all samples mimic the native tendon anisotropic and hierarchical structure (Figure 2A-F). The diameters of yarns and nanofibers measured from SEM micrographs of uncoated samples were 149±16 μm (Figure 2A) and 134±28 nm (Figure 2D), respectively, and in agreement with our previously reported data.[11] These dimensions are within the range of collagen fascicles

(150-1000 μm) and fibrils (20-150 nm) of the native tissue,[1] which is worthwhile because previous studies using biomimetic fibrillar scaffolds for tendon tissue engineering have positively correlated these parameters with tenogenic cell fate and regenerative responses.[8,38] The coatings did not alter the average diameter of the yarns, but slightly increased the diameter of the nanofibers (144±32 and 153±33 nm, for the PDA and TROPO/PDA coated yarns, Figure S2), while remaining in the range of the native collagen fibrils. The influence of the coatings on the roughness of the samples was studied using AFM; the incorporation of PDA and TROPO in the scaffolds did not significantly alter surface roughness, despite the presence of self-polymerized PDA aggregates on the surface of a ~10 nm thick uniform layer of PDA, as commonly observed in other PDA coated biomaterial surfaces.[39]

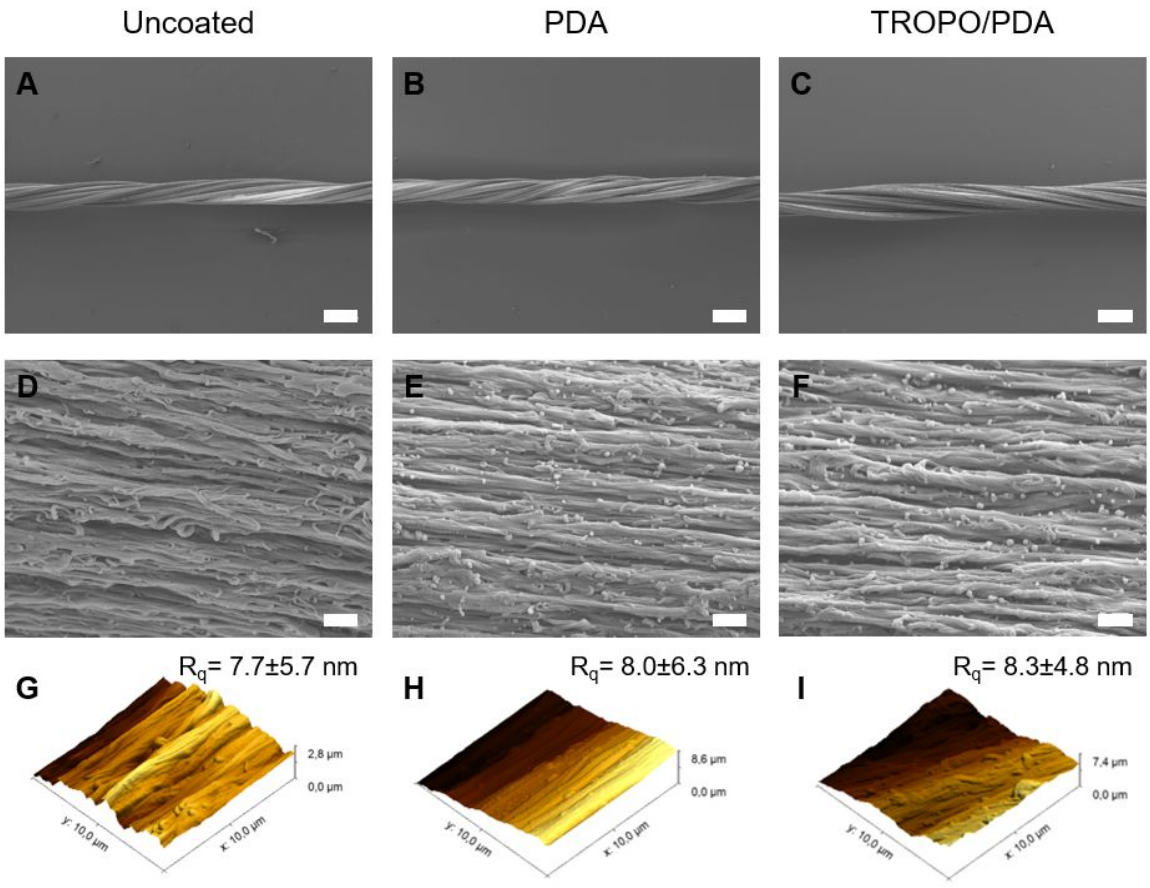

Figure 2. Morphological characterization of developed tendon mimetic constructs. SEM micrographs with low (A-C, scale bar: 200 µm) and high (D-F, scale bar: 2 µm) magnifications and AFM 3D projections (G-I) of uncoated, PDA-coated and TROPO/PDA-coated yarns with respective average root-mean-square roughness (Rq).

The success of the PDA coating was confirmed by FTIR and Raman spectroscopy (Figure S3A and B) and the binding of TROPO was evaluated by subtracting the FTIR spectra of the background material from the corresponding TROPO-coated samples

(Figure 3A). The resulting spectra present two well defined peaks in the presence of PDA, at 1629 and 1517 cm^{-1}, each corresponding to the distinctive amides I and II of TROPO, detected in its individual spectrum.[28] To evaluate the extent of TROPO physical adsorption on the yarns and the importance of PDA as an intermediate for its covalent immobilization on the biomaterial surface, uncoated yarns incubated with TROPO solutions were also analyzed. In the absence of PDA, the amide peaks, resulting from spectra subtraction, were not as well defined, and their intensity was lower than on PDA-coated samples, suggesting inferior protein retention (Figure 3A). As a result, the nature of these chemical interactions was investigated by determining the relative amount of TROPO that remains linked to the scaffold after a warm SDS wash (Figure S3 C). Prior to washing, the uncoated and PDA-coated samples exhibited similar protein retention, however following the detergent washing step, the majority of TROPO (88%) was removed from the uncoated samples, whereas only 23% was washed from PDA-coated yarns. These results further support the existence of a covalent grafting of TROPO on the PDA-coated surfaces, that can proceed via Michaels' addition and/or Schiff-base reactions,[40] as opposed to its simple physisorption on the uncoated substrates. On this basis, the reactive quinone species of PDA preferentially reacted with amines in lysine residues distributed throughout the TROPO, rather than with its two closely-spaced cysteine residues that form a disulfide bond.[41] This mode of attachment contributes to a random distribution of the cell interactive C-terminus on the surfaces of the yarns. In

addition, we performed TROPO coatings using Tris buffer (no NaCl, pH 8.5), which supported these types of bonds between PDA and TROPO as these are favored by the formation of reactive quinone species in PDA at alkaline pH and stabilized by Tris amines.[37] These conditions do not impair protein functionality, as demonstrated in previous studies where TROPO surface coatings were performed without salt and pH 11.5.[27]

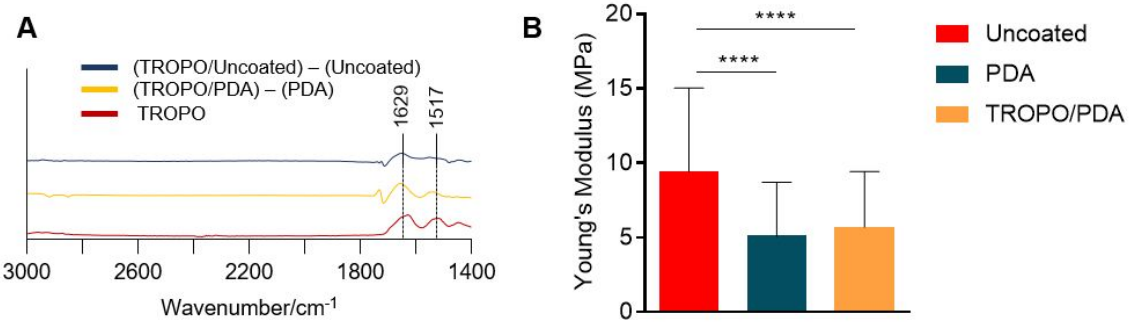

Figure 3. Physical and chemical characterization of coatings. A) FTIR spectra obtained by subtracting the material spectra from the respective TROPO-coated samples and TROPO spectrum; and B) Stiffness of the substrate determined through nanoindentation AFM before and after PDA- and TROPO/PDA-coating. Statistical differences: ****$p<0.0001$.

In order to study the impact of the coating steps on each scaffold's stiffness at the nanoscale, which would be experienced by cells, we performed AFM nanoindentation measurements in the different hydrated samples under physiological conditions. We found that the PDA and TROPO coatings significantly decreased the stiffness of the

scaffold's surface from 9.0±4.8 MPa in the bare samples to 4.7±3.0 MPa and 5.6±3.6 MPa after the PDA coating and TROPO immobilization, respectively (Figure 3B). Remarkably, the stiffness of PDA and TROPO coated samples are of the same order as a hydrated bovine Achilles tendon (2 to 5 MPa), determined using similar nanoindentation and conditions.[42] In a previous study, surface stiffness tuned to this range (3.5 MPa) led to an upregulation of tenomodulin (TNMD) expression when compared with significantly softer surfaces (0.35 MPa).[43]

Cell interaction with the biomimetic substrates. The morphology of hASCs on the different substrates was evaluated using confocal microscopy after 5 days of culture. Figure 4A shows that adhered hASCs were elongated and spread in a preferential axis direction, along the length of the yarns. These results are consistent with the well-known cell contact guidance effect of substrates with anisotropic micro and nano topographies that in general induces cell elongation with high degrees of alignment.[8,9] Moreover, images revealed that hASCs presented a more pronounced spindle-shape fibroblast-like morphology characteristic of tenocytes[44] in the presence of TROPO, markedly after 5 days of culture. These findings were confirmed by determining the nuclei aspect ratio (AR) (Figure 4B), a parameter related with cell shape.[12] AR was significantly higher in the presence of TROPO (2.48 ± 0.8), compared to the uncoated and PDA-coated conditions (1.87 ± 0.5 and 2.05 ± 0.5 respectively), indicating that the surface properties sensed by

hASCs result in actin filaments arrangement, which affect their shape. Hence, considering that in previous studies fibroblasts exhibited higher AR on stiff substrates than on soft substrates,[12] the increased AR on our TROPO/PDA samples after 5 days was probably driven by their initial cell-TROPO interactions. Cells are able to bind to the C-terminus and the central region of the elastin precursor, using integrin αVβ3 and αVβ5, respectively.[45,46] This is worthwhile because tropoelastin-integrin crosstalk activates the mechanosensing pathways that result in enhanced cell focal adhesion and cytoskeleton organization.[26] Still, these differences in AR were no longer observed after 14 days (Figure 4B). While the AR of cells on TROPO remained unchanged from day 5 to 14, it significantly increased on uncoated and PDA-coated samples. In addition, cell cytoskeleton directionality analysis showed that cells align with the yarns nanotopography and presented similar directional distribution for the different groups after 14 and 21 days (Figure S4 A and B). These results suggest that cells reacted to the nanotopographical cues of the underlying substrate, acquiring a tenocyte-like morphology,[44] while emphasizing the role of TROPO on promoting early and fast cell elongation, which could impact tenogenic differentiation of stem cells, as previously reported.[13] Cell proliferation was studied by DNA quantification from cell lysates (Figure 4C); although PDA-coated yarns exhibit a catechol- and amine-rich highly hydrophilic layer that presents reactivity towards cells,[47] and TROPO is known to enhance cell

proliferation,[48] the inherent biomimetic nature of our yarns allowed for a fast proliferation from 5 to 14 days of culture, with similar behavior across the conditions.

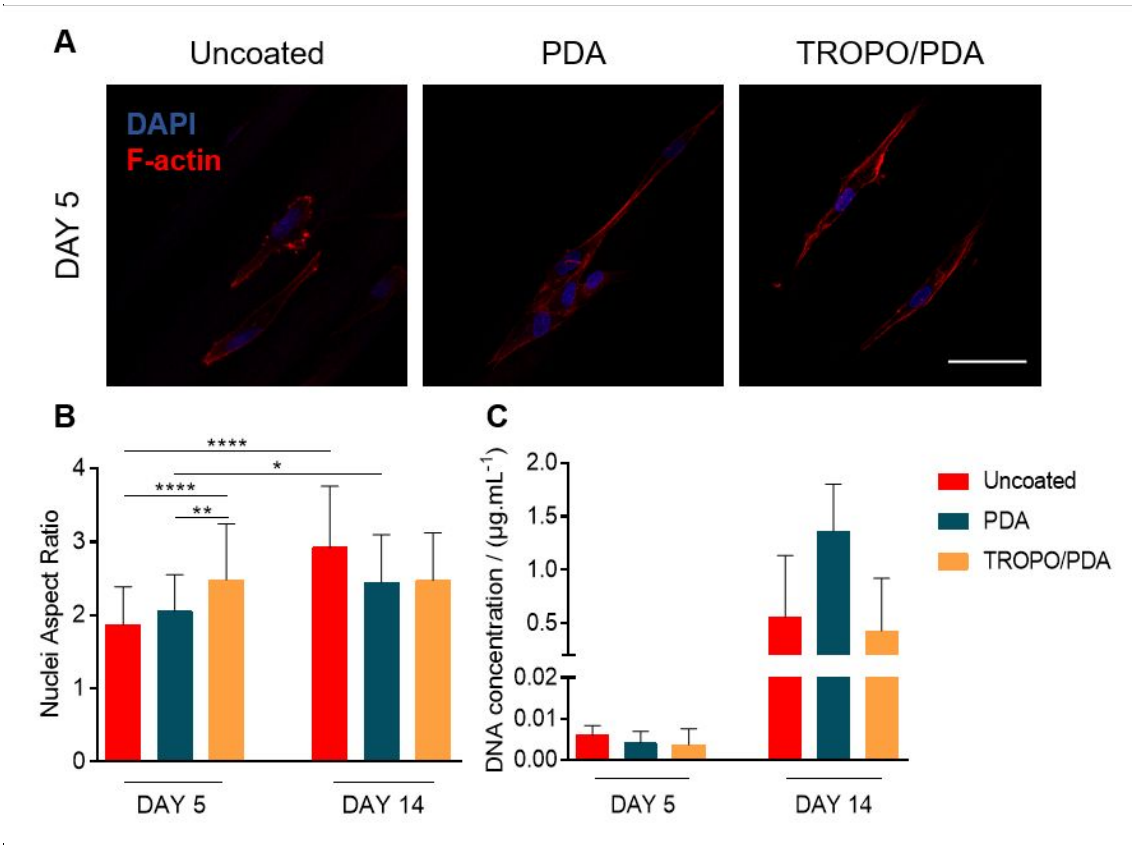

Figure 4. Morphometric analysis and cell proliferation evaluation of biomimetic yarns seeded with cells: A) High magnification confocal images of hASCs nuclei (blue) and actin filaments (red) organization on uncoated, PDA-coated and TROPO/PDA-coated yarns after 5 days of culture. Scale bar: 50 µm; B) Nuclei aspect ratio of hASCs at 5 days and 14 days of culture. Statistical differences: *p<0.05; ***p<0.001; ****p<0.0001; and C) Cell proliferation of seeded hASCs through DNA quantification after 5 and 14 days in culture.

Tenogenic commitment by hASCs in biomimetic constructs. To study the tenogenic commitment of hASCs, two of the most widely accepted tenogenic markers scleraxis (SCX) and TNMD,[3] were assessed by immunocytochemistry. Figure 5A evidences a similar profile of SCX expression concentrated in the nuclei in all conditions after 14 days of culture, which was in accordance with the gene expression analysis (Figure S5). This expression was maintained up to 21 days in PDA and TROPO substrates, while it significantly decreased on the uncoated samples (Figure 5B). Likewise, TNMD expression at day 14 was similar for all the groups, which was maintained up to 21 days of culture (Figure 5C). While SCX is a transcription factor expressed mainly during early tendon development and present in mature tendons,[3,49] TNMD is a downstream transmembrane protein expressed by tenocytes responsible for the proliferation and maturation of tendon ECM.[50,51] Thus, we hypothesize that the lower surface stiffness of the PDA and TROPO/PDA-coated samples activated mechanotransduction pathways that resulted in the higher and prolonged expression of SCX, ensuring their sustained commitment towards the tenogenic lineage. This increased the expression of the late tenogenic marker TNMD on the coated samples after 21 days of culture. These results suggest that the commitment of hASCs towards the tenogenic lineage might be mainly driven by the biophysical characteristics of the yarns, i.e. their nanotopography, hierarchical architecture and stiffness.

In addition, to evaluate the unintended trans-differentiation of hASCs, we analyzed the expression of the pre-osteogenic gene runt-related transcription factor 2 (RUNX2) and the myofibroblast marker alpha smooth muscle actin (ACTA2) (Figure 5E). In particular, the expression of RUNX2 was downregulated and significantly decreased for TROPO/PDA scaffolds, which is consistent with a combined effect of suitable surface elasticity (closer to the native tissue), nanotopographic cues and biological signaling. Interestingly, Islam *et al.* reported an increased expression of tendon-related markers by increasing the stiffness of collagen membranes, but this effect was also accompanied by a simultaneous upregulation and increased expression of *RUNX2*.[52] A recent study reported, however, that the differentiation of tendon-derived stem cells into the tenogenic lineage was inhibited by increasing the stiffness of gelatin hydrogels.[53] Even though the direct comparison between works should be made with caution due to differences in their chemical nature and topography, the diverse cell responses highlight the importance of the adequate combination of biophysical and biochemical cues to achieve tenogenic commitment of stem cells. Additionally, ACTA2, a fibrosis-associated gene also related to myofibroblast differentiation, and which leads to scar tissue formation with continuous upregulation,[54] was downregulated on TROPO/PDA compared with PDA coatings. We propose that the nature of PDA coating induces an unintended more pro-osteogenic and even pro-fibrotic cell phenotype, which is counterbalanced by the presence of TROPO. On the other hand, although TROPO has been associated with cell

stemness maintenance, either surface-bound or as a culture medium supplement,[26] here, TROPO-coated samples are clearly not impairing the tenogenic commitment. Therefore, we hypothesize that when combined with the appropriate biophysical cues, namely biomimetic nanotopography and lower stiffness, TROPO is able to foster and sustain the tenogenic differentiation of hASCs. Additional studies should be conducted to further understand this mechanism.

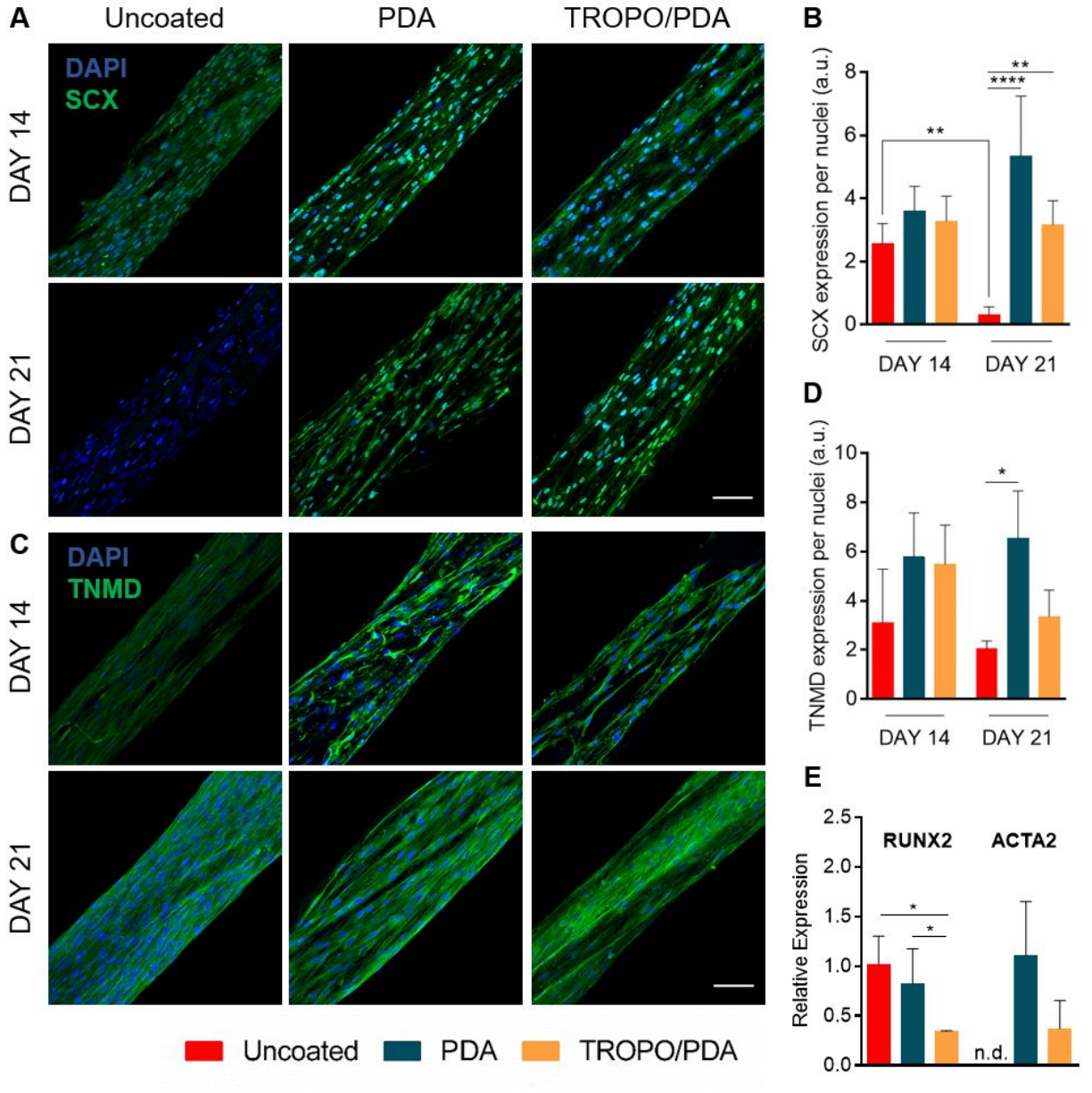

Figure 5. Expression of key tenogenic markers by hASCs on the biomimetic constructs. A and C) Confocal images of immunolabeled samples against the transcription factor SCX (green) and the transmembrane protein TNMD (green) expressed by hASCs after 14 and 21 days of culture, counterstained with cells nuclei (blue). Scale bar: 100 μm; B and D) Area of SCX and TNMD staining (green) normalized by area of cell nuclei (blue); and

E) Gene expression analysis of other non-related markers *RUNX2* and *ACTA2* after 14 days of culture (n.d., not detected). Normalization was performed to *GAPDH* and *ACTB* and data presented relative to control yarns. Statistical differences: *p<0.05; **p<0.01; ****p<0.0001.

ECM synthesis by hASCs in developed constructs. To evaluate the impact of the coatings on the synthesis and organization of ECM, we assessed a range of key tendon ECM components, i.e. fibrillar proteins collagen type I (COLI), type III (COL3a1) and elastin (ELN), the proteoglycan decorin (DCN), and the glycoprotein tenascin (TNC). By qPCR analysis, we observed that *COL3a1* and *DCN* were similarly expressed between conditions after 14 days of culture (Figure 6A). This early expression of both markers is important for later COLI normal fibrillogenesis, thinning and alignment,[1,4] which allows the characteristic tendon strength and elasticity.[55,56] Next, the expression of COLI and TNC was assessed through immunocytochemistry after 21 days of culture. Figure 6B and D show that cells synthesized and deposited their own ECM containing TNC and COLI, with TNC being significantly more prominent in the TROPO/PDA-coated samples (Figure 6C) and COLI being equally expressed in the different groups (Figure 6D).These proteins appropriately followed the orientation and nanotopography of the yarns (Figure S4 D and E), mimicking native tendon ECM anisotropy, which is critical for tendon function.[1] Both markers are widely studied in the tendon tissue engineering field; while

COLI is the main component of tendons, TNC provides extensibility and flexibility for the tissue.[57]

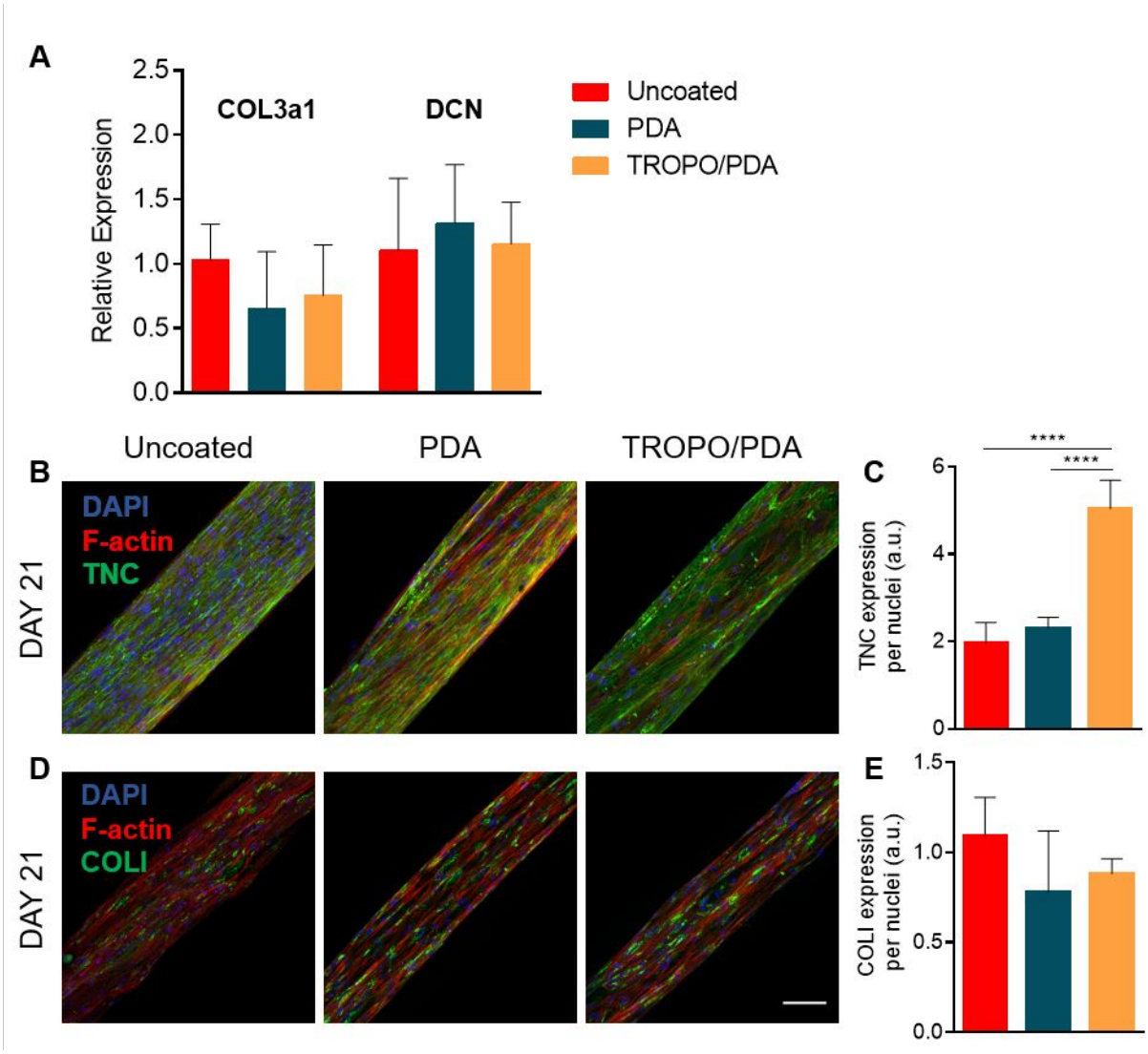

Figure 6. Expression of ECM markers by hASCs on the biomimetic constructs. A) Gene expression analysis of tendon-related ECM markers *COL3a1* and *DCN* after 14 days of culture. Normalization was performed to *GAPDH* and *ACTB* and data presented relative to uncoated yarns; B and D) Confocal images of immunolabeled samples against the ECM proteins TNC (green) and COLI (green) expressed by hASCs after 21 days of culture with

cells nuclei (blue) and cytoskeleton (red). Scale bar: 100 μm; and C and E) Area of TNC and COLI staining (green) normalized by area of cell nuclei (blue). Statistical differences: ****$p<0.0001$.

In order to analyze the effect of TROPO coating as a trigger for elastin synthesis by hASCs, we analyzed gene expression and protein after 14 and 21 days of culture (Figure 7A and C). While on uncoated and PDA samples, cells were not able to synthesize and deposit elastic fibers, cells on TROPO/PDA-coated samples showed an upregulation of the elastin gene at day 14, accompanied by an increased synthesis and deposition of the protein, as evidenced by the immunolabeled images. Furthermore, elastin presented a typical fibrillar morphology interspersed within other ECM proteins, along the length of the yarns and in between cells.[18,22,58] This observation was further confirmed by the quantification of the area of the yarn specifically stained with anti-elastin antibody (Figure 7B). We found that this was significantly smaller for the uncoated and PDA-coated samples than for the TROPO/PDA-coated yarns; indeed TROPO/PDA-coated yarns showed a 2.1-fold increase in TROPO deposition at day 14 and a 15.2-fold increase at day 21, when compared to the uncoated yarns. Although some staining was observed for these samples, we attribute this to autofluorescence and/or background caused by non-specific dye absorption rather than elastin synthesis. Elastic fiber assembly relies on

the progressive binding of the secreted TROPO to cells receptors, macromolecular assembly (coacervation) and organization in the ECM space with the intervention of microfibrillar proteins followed by crosslinking of occasionally oxidized lysine residues, a process that can take around 12-14 days.[59] Here, the increased elastin gene and protein expression after 14 days observed for cells on TROPO/PDA yarns indicates that cells synthesized their own TROPO or utilized TROPO that was released from the yarn surface over time (Figure S6). We note that PDA-coated yarns expressed basal elastin mRNA levels but did not show protein staining, so an interplay between *de novo* elastin synthesis and deposition of released TROPO might have occurred. Previous studies have added TROPO to the cell culture medium to promote elastogenesis.[7,18] To our knowledge this is the first study to suggest that TROPO coatings can contribute to the synthesis of elastin regardless of the elastogenic nature of the cells,[27,28,58] a topic that requires further investigation. Nanomechanical properties of the deposited ECM at the surfaces of the yarns were determined at day 21 of culture through AFM nanoidentation (Figure 7D). We observed a tendency for the deposition of a stiffer matrix on top of the uncoated yarns (19.4 ± 12.5 kPa), compared to the PDA-coated (11.5 ± 6.9 kPa) and the TROPO/PDA-coated yarns (9.8 ± 5.9 kPa), although the high variability suggests nonuniform ECM synthesis. Moreover, the differences between PDA and TROPO/PDA samples were small, indicating that the underlying surface stiffness might have played a role in the mechanical properties of the newly synthesized ECM. The process of matrix remodeling

is highly dynamic and continuous, and we only evaluated the nanomechanical properties, thus it would be worthwhile to further explore its progression and correlate it with cell phenotype so new insights regarding mechanotransduction mechanisms could be achieved. It is worth emphasizing that for the first time TROPO-coated biomimetic yarns enhanced the deposition of tendon-like matrix containing elastin, which in the long-term has the potential to impact positively on the maintenance of the tenogenic phenotype and the development of a successful tendon tissue engineering strategy.

During morphogenesis, it is known that mechanical cues can be propagated over long distances more rapidly than biochemical cues and that the transmission of forces in highly elastic substrates is faster than in stiffer ones.[60] Consequently, considering the mechanosensitive profile of tendons, the incorporation of a bioreactor for load application in the developed scaffolds might be another interesting approach to study tendon ECM remodeling.[61] In this study, we envision the use of scaffolds seeded with cells for tendon regeneration and on that basis, we showed that hASCs cultured on TROPO-coated tendon biomimetic scaffolds were able to acquire a phenotype that is closer to the one from native tendon cells.[9,44] Furthermore, the ability of TROPO-coated substrates to recruit stem cells[26] might augment the value of TROPO/PDA-coated woven scaffolds in acellular strategies to attract resident stem cells.

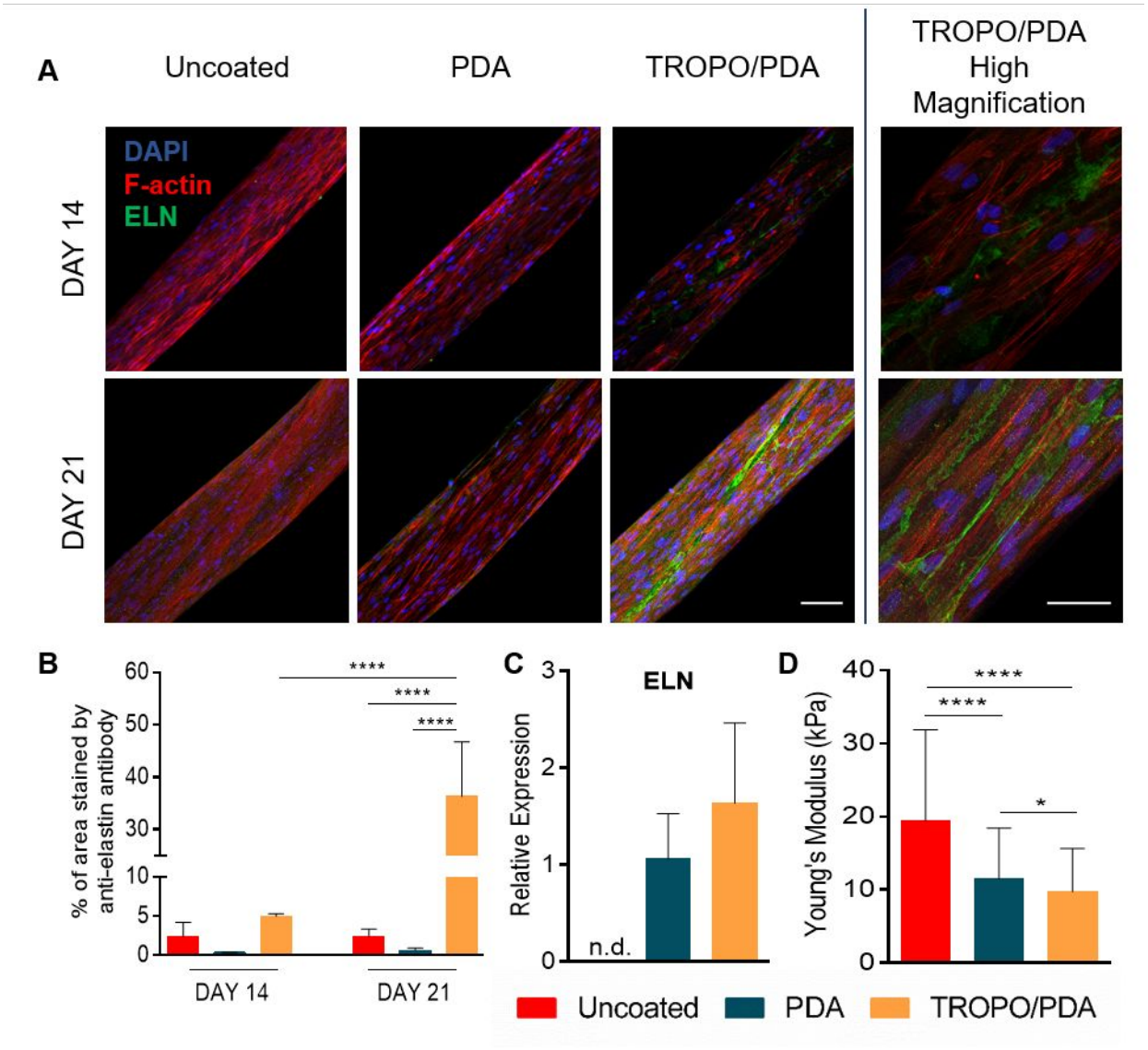

Figure 7. Evaluation of the expression and deposition of elastin by hASCs on the biomimetic constructs. A) Confocal images of immunolabeled samples against the ECM protein ELN (green) expressed by hASCs after 14 and 21 days of culture, with stained nuclei (blue) and cytoskeletons (red). Scale bar low and high magnifications: 100 μm and 50 μm, respectively; B) Gene expression analysis of ECM marker *ELN* after 14 days of culture (n.d., not detected). Normalization was performed to *GAPDH* and *ACTB* and data

presented relative to PDA-coated yarns; C) Percentage of yarn area stained by the anti-elastin antibody after 14 and 21 days of culture; and D) Young's Modulus of the deposited ECM at the surface of the yarns after 21 days of culture. Statistical differences: *$p<0.05$; ****$p<0.0001$.

CONCLUSIONS

We successfully developed tendon biomimetic scaffolds by recreating its native architecture, at the nano to macro scale, while providing necessary biochemical cues to trigger and maintain the tenogenic phenotype. We achieved this using a simple dip-coat method. Tropoelastin coatings promoted faster cell elongation, sustained the tenogenic commitment of stem cells and allowed the autologous synthesis of a tendon-like ECM rich in elastin by differentiated cells. The possibility of generating 3D hierarchical and personalized scaffolds from the yarns through weaving techniques widens the range of potential applications. Constructs can be tuned to patient defects, and since tropoelastin is well tolerated in the medical field, the developed scaffolds are attractively closer to clinical implementation. Moreover, by generating a more realistic ECM, the same yarns have the potential of being used as models to screen inflammatory responses and study the mechanisms that drive tenogenesis. In summary, the combination of tropoelastin with the nanotopography of the scaffolds modulated stem cell fate towards tenogenic differentiation and the production of a tendon-mimetic ECM.

ASSOCIATED CONTENT

Supporting Information.

The following files are available free of charge: Synthesis of CNCs and characterization. Chitosan purification. Surface characterization of the coatings. Directionality analysis. Real-time PCR primers and SCX mRNA levels. Tropoelastin release from the yarns.

AUTHOR INFORMATION

Corresponding Authors

*Manuel Gómez-Florit: mgflorit@i3bs.uminho.pt

*Manuela E. Gomes: megomes@i3bs.uminho.pt

Author Contributions

The manuscript was written through contributions of all authors. All authors have given approval to the final version of the manuscript.

Notes

A.S.W. is the founding scientist of Elastagen Pty. Ltd., now sold to Allergan, Inc.

ACKNOWLEDGMENTS

The authors acknowledge the European Union's Horizon 2020 research and innovation program under the Marie Sklodowska-Curie grant agreement No 706996, Teaming grant agreement No 739572 – The Discoveries CTR, European Research Council grant agreement No 726178, and ERA Chair grant agreement No 668983 - FORECAST; Biomedical Engineering Australian Mobility (BEAM) Program – Master Joint Mobility Project between EU Commission Australian Government; Fundação para a Ciência e a Tecnologia (FCT) for Post-Doc grant SFRH/BPD/112459/2015 and project SmarTendon (PTDC/NAN-MAT/30595/2017); Norte Portugal Regional Operational Program (NORTE 2020), under the PORTUGAL 2020 Partnership Agreement, through the European Regional Development Fund for NORTE-01-0145-FEDER-000021. This research was facilitated by access to Sydney Analytical, a core research facility at the University of Sydney. Hospital da Prelada (Portugal) is as well acknowledged for providing the tissue samples.

REFERENCES

(1) Docheva, D.; Müller, S. A.; Majewski, M.; Evans, C. H. Biologics for Tendon Repair. *Adv. Drug Deliv. Rev.* **2015**, *84*, 222–239. https://doi.org/10.1016/j.addr.2014.11.015.

(2) Liu, Y.; Ramanath, H. S.; Wang, D. A. Tendon Tissue Engineering Using Scaffold

Enhancing Strategies. *Trends Biotechnol.* **2008**, *26* (4), 201–209. https://doi.org/10.1016/j.tibtech.2008.01.003.

(3) Gaut, L.; Duprez, D. Tendon Development and Diseases. *Wiley Interdiscip. Rev. Dev. Biol.* **2016**, *5* (1), 5–23. https://doi.org/10.1002/wdev.201.

(4) Wang, J. H. C. Mechanobiology of Tendon. *J. Biomech.* **2006**, *39* (9), 1563–1582. https://doi.org/10.1016/j.jbiomech.2005.05.011.

(5) Yeo, G. C.; Mithieux, S. M.; Weiss, A. S. The Elastin Matrix in Tissue Engineering and Regeneration. *Curr. Opin. Biomed. Eng.* **2018**, *6*, 27–32. https://doi.org/10.1016/j.cobme.2018.02.007.

(6) Miranda-Nieves, D.; Chaikof, E. L. Collagen and Elastin Biomaterials for the Fabrication of Engineered Living Tissues. *ACS Biomater. Sci. Eng.* **2017**, *3* (5), 694–711. https://doi.org/10.1021/acsbiomaterials.6b00250.

(7) Mithieux, S. M.; Weiss, A. S. Design of an Elastin-Layered Dermal Regeneration Template. *Acta Biomater.* **2017**, *52*, 33–40. https://doi.org/10.1016/j.actbio.2016.11.054.

(8) Erisken, C.; Zhang, X.; Moffat, K. L.; Levine, W. N.; Lu, H. H. Scaffold Fiber Diameter Regulates Human Tendon Fibroblast Growth and Differentiation. *Tissue Eng. Part A* **2013**, *19* (3–4), 519–528. https://doi.org/10.1089/ten.tea.2012.0072.

(9) Yin, Z.; Chen, X.; Chen, J. L.; Shen, W. L.; Hieu Nguyen, T. M.; Gao, L.; Ouyang, H. W. The Regulation of Tendon Stem Cell Differentiation by the Alignment of Nanofibers. *Biomaterials* **2010**, *31* (8), 2163–2175. https://doi.org/10.1016/j.biomaterials.2009.11.083.

(10) Younesi, M.; Islam, A.; Kishore, V.; Anderson, J. M.; Akkus, O. Tenogenic Induction of Human MSCs by Anisotropically Aligned Collagen Biotextiles. *Adv. Funct. Mater.* **2014**, *24* (36), 5762–5770. https://doi.org/10.1002/adfm.201400828.

(11) Laranjeira, M.; Domingues, R. M. A.; Costa-Almeida, R.; Reis, R. L.; Gomes, M. E. 3D Mimicry of Native-Tissue-Fiber Architecture Guides Tendon-Derived Cells and Adipose Stem Cells into Artificial Tendon Constructs. *Small* **2017**, *13* (31), 1700689. https://doi.org/10.1002/smll.201700689.

(12) Yu, H.; Lim, K. P.; Xiong, S.; Tan, L. P.; Shim, W. Functional Morphometric Analysis in Cellular Behaviors: Shape and Size Matter. *Adv. Healthc. Mater.* **2013**, *2* (9), 1188–1197. https://doi.org/10.1002/adhm.201300053.

(13) Lin, J.; Zhou, W.; Han, S.; Bunpetch, V.; Zhao, K.; Liu, C.; Yin, Z.; Ouyang, H. Cell-Material Interactions in Tendon Tissue Engineering. *Acta Biomater.* **2018**, *70*, 1–11. https://doi.org/10.1016/j.actbio.2018.01.012.

(14) Ozsvar, J.; Mithieux, S. M.; Wang, R.; Weiss, A. S. Elastin-Based Biomaterials and

Mesenchymal Stem Cells. *Biomater. Sci.* **2015**, *3* (6), 800–809. https://doi.org/10.1039/C5BM00038F.

(15) Pang, X.; Wu, J.-P.; Allison, G. T.; Xu, J.; Rubenson, J.; Zheng, M.-H.; Lloyd, D. G.; Gardiner, B.; Wang, A.; Kirk, T. B. Three Dimensional Microstructural Network of Elastin, Collagen, and Cells in Achilles Tendons. *J. Orthop. Res.* **2017**, *35* (6), 1203–1214. https://doi.org/10.1002/jor.23240.

(16) Pezzoli, D.; Di Paolo, J.; Kumra, H.; Fois, G.; Candiani, G.; Reinhardt, D. P.; Mantovani, D. Fibronectin Promotes Elastin Deposition, Elasticity and Mechanical Strength in Cellularised Collagen-Based Scaffolds. *Biomaterials* **2018**, *180*, 130–142. https://doi.org/10.1016/j.biomaterials.2018.07.013.

(17) Wise, S. G.; Mithieux, S. M.; Weiss, A. S. Engineered Tropoelastin and Elastin-Based Biomaterials. *Adv. Protein Chem. Struct. Biol.* **2009**, *78* (09), 1–24. https://doi.org/10.1016/S1876-1623(08)78001-5.

(18) Yeo, G. C.; Tarakanova, A.; Baldock, C.; Wise, S. G.; Buehler, M. J.; Weiss, A. S. Subtle Balance of Tropoelastin Molecular Shape and Flexibility Regulates Dynamics and Hierarchical Assembly. *Sci. Adv.* **2016**, *2* (2), e1501145. https://doi.org/10.1126/sciadv.1501145.

(19) Sato, F.; Seino-Sudo, R.; Okada, M.; Sakai, H.; Yumoto, T.; Wachi, H. Lysyl Oxidase

Enhances the Deposition of Tropoelastin through the Catalysis of Tropoelastin Molecules on the Cell Surface. *Biol. Pharm. Bull.* **2017**, *40* (10), 1646–1653. https://doi.org/10.1248/bpb.b17-00027.

(20) Aya, R.; Ishiko, T.; Noda, K.; Yamawaki, S.; Sakamoto, Y.; Tomihata, K.; Katayama, Y.; Yoshikawa, K.; Kubota, H.; Nakamura, T.; Naitoh, M.; Suzuki, S. Regeneration of Elastic Fibers by Three-Dimensional Culture on a Collagen Scaffold and the Addition of Latent TGF-β Binding Protein 4 to Improve Elastic Matrix Deposition. *Biomaterials* **2015**, *72*, 29–37. https://doi.org/10.1016/j.biomaterials.2015.08.036.

(21) Annabi, N.; Mithieux, S. M.; Weiss, A. S.; Dehghani, F. Cross-Linked Open-Pore Elastic Hydrogels Based on Tropoelastin, Elastin and High Pressure CO2. *Biomaterials* **2010**, *31* (7), 1655–1665. https://doi.org/10.1016/j.biomaterials.2009.11.051.

(22) Annabi, N.; Rana, D.; Shirzaei Sani, E.; Portillo-Lara, R.; Gifford, J. L.; Fares, M. M.; Mithieux, S. M.; Weiss, A. S. Engineering a Sprayable and Elastic Hydrogel Adhesive with Antimicrobial Properties for Wound Healing. *Biomaterials* **2017**, *139*, 229–243. https://doi.org/10.1016/j.biomaterials.2017.05.011.

(23) Hu, X.; Park, S. H.; Gil, E. S.; Xia, X. X.; Weiss, A. S.; Kaplan, D. L. The Influence of Elasticity and Surface Roughness on Myogenic and Osteogenic-Differentiation of Cells on Silk-Elastin Biomaterials. *Biomaterials* **2011**, *32* (34), 8979–8989.

https://doi.org/10.1016/j.biomaterials.2011.08.037.

(24) Nivison-Smith, L.; Rnjak, J.; Weiss, A. S. Synthetic Human Elastin Microfibers: Stable Cross-Linked Tropoelastin and Cell Interactive Constructs for Tissue Engineering Applications. *Acta Biomater.* **2010**, *6* (2), 354–359. https://doi.org/10.1016/j.actbio.2009.08.011.

(25) Machula, H.; Ensley, B.; Kellar, R. Electrospun Tropoelastin for Delivery of Therapeutic Adipose-Derived Stem Cells to Full-Thickness Dermal Wounds. **2014**, *3* (5), 367–375. https://doi.org/10.1089/wound.2013.0513.

(26) Yeo, G. C.; Weiss, A. S. Soluble Matrix Protein Is a Potent Modulator of Mesenchymal Stem Cell Performance. *Proc. Natl. Acad. Sci.* **2019**, *116* (6), 2042–2051. https://doi.org/10.1073/pnas.1812951116.

(27) Yeo, G. C.; Kondyurin, A.; Kosobrodova, E.; Weiss, A. S.; Bilek, M. M. M. A Sterilizable, Biocompatible, Tropoelastin Surface Coating Immobilized by Energetic Ion Activation. *J. R. Soc. Interface* **2017**, *14* (127), 20160837. https://doi.org/10.1098/rsif.2016.0837.

(28) Landau, S.; Szklanny, A. A.; Yeo, G. C.; Shandalov, Y.; Kosobrodova, E.; Weiss, A. S.; Levenberg, S. Tropoelastin Coated PLLA-PLGA Scaffolds Promote Vascular Network Formation. *Biomaterials* **2017**, *122*, 72–82.

https://doi.org/10.1016/j.biomaterials.2017.01.015.

(29) Oshima, Y.; Shukunami, C.; Honda, J.; Nishida, K.; Tashiro, F.; Miyazaki, J. ichi; Hiraki, Y.; Tano, Y. Expression and Localization of Tenomodulin, a Transmembrane Type Chondromodulin-I-Related Angiogenesis Inhibitor, in Mouse Eyes. *Investig. Ophthalmol. Vis. Sci.* **2003**, *44* (5), 1814–1823. https://doi.org/10.1167/iovs.02-0664.

(30) Domingues, R. M. A.; Chiera, S.; Gershovich, P.; Motta, A.; Reis, R. L.; Gomes, M. E. Enhancing the Biomechanical Performance of Anisotropic Nanofibrous Scaffolds in Tendon Tissue Engineering: Reinforcement with Cellulose Nanocrystals. *Adv. Healthc. Mater.* **2016**, *5* (11), 1364–1375. https://doi.org/10.1002/adhm.201501048.

(31) Khil, M. S.; Bhattarai, S. R.; Kim, H. Y.; Kim, S. Z.; Lee, K. H. Novel Fabricated Matrix via Electrospinning for Tissue Engineering. *J. Biomed. Mater. Res. - Part B Appl. Biomater.* **2005**, *72* (1), 117–124. https://doi.org/10.1002/jbm.b.30122.

(32) Lee, H.; Dellatore, S. M.; Miller, W. M.; Messersmith, P. B. Mussel-Inspired Surface Chemistry for Multifunctional Coatings. *Science (80-.).* **2007**, *318* (5849), 426–430. https://doi.org/10.1126/science.1147241.

(33) Martin, S. L.; Vrhovski, B.; Weiss, A. S. Total Synthesis and Expression in Escherichia Coli of a Gene Encoding Human Tropoelastin. *Gene* **1995**, *154* (2), 159–

166. https://doi.org/10.1016/0378-1119(94)00848-M.

(34) Carvalho, P. P.; Wu, X.; Yu, G.; Dias, I. R.; Gomes, M. E.; Reis, R. L.; Gimble, J. M. The Effect of Storage Time on Adipose-Derived Stem Cell Recovery from Human Lipoaspirates. *Cells Tissues Organs* **2011**, *194* (6), 494–500. https://doi.org/10.1159/000324892.

(35) Mendes, B. B.; Gómez-Florit, M.; Pires, R. A.; Domingues, R. M. A.; Reis, R. L.; Gomes, M. E. Human-Based Fibrillar Nanocomposite Hydrogels as Bioinstructive Matrices to Tune Stem Cell Behavior. *Nanoscale* **2018**, 17388–17401. https://doi.org/10.1039/C8NR04273J.

(36) Waite, J. H. Surface Chemistry: Mussel Power. *Nat. Mater.* **2008**, *7* (1), 8–9. https://doi.org/10.1038/nmat2087.

(37) Barclay, T. G.; Hegab, H. M.; Clarke, S. R.; Ginic-Markovic, M. Versatile Surface Modification Using Polydopamine and Related Polycatecholamines: Chemistry, Structure, and Applications. *Adv. Mater. Interfaces* **2017**, *4* (19), 1–38. https://doi.org/10.1002/admi.201601192.

(38) Gilchrist, C. L.; Ruch, D. S.; Little, D.; Guilak, F. Micro-Scale and Meso-Scale Architectural Cues Cooperate and Compete to Direct Aligned Tissue Formation. *Biomaterials* **2014**, *35* (38), 10015–10024.

https://doi.org/10.1016/j.biomaterials.2014.08.047.

(39) Ding, Y.; Weng, L.; Yang, M.; Yang, Z.; Lu, X.; Huang, N.; Leng, Y. Insights into Aggregation / Deposition and Structure of Polydopamine Film. *Langmuir* **2014**, *30* (40). https://doi.org/10.1021/la5026608.

(40) Ryu, J. H.; Messersmith, P. B.; Lee, H. Polydopamine Surface Chemistry: A Decade of Discovery. *ACS Appl. Mater. Interfaces* **2018**, *10* (9), 7523–7540. https://doi.org/10.1021/acsami.7b19865.

(41) Wise, S. G.; Yeo, G. C.; Hiob, M. A.; Rnjak-Kovacina, J.; Kaplan, D. L.; Ng, M. K. C.; Weiss, A. S. Tropoelastin: A Versatile, Bioactive Assembly Module. *Acta Biomater.* **2014**, *10* (4), 1532–1541. https://doi.org/10.1016/j.actbio.2013.08.003.

(42) Grant, C. A.; Brockwell, D. J.; Radford, S. E.; Thomson, N. H. Tuning the Elastic Modulus of Hydrated Collagen Fibrils. *Biophys. J.* **2009**, *97* (11), 2985–2992. https://doi.org/10.1016/j.bpj.2009.09.010.

(43) Tong, W. Y.; Shen, W.; Yeung, C. W. F.; Zhao, Y.; Cheng, S. H.; Chu, P. K.; Chan, D.; Chan, G. C. F.; Cheung, K. M. C.; Yeung, K. W. K.; Lam, Y. W. Functional Replication of the Tendon Tissue Microenvironment by a Bioimprinted Substrate and the Support of Tenocytic Differentiation of Mesenchymal Stem Cells. *Biomaterials* **2012**, *33* (31), 7686–7698.

https://doi.org/10.1016/j.biomaterials.2012.07.002.

(44) Spanoudes, K.; Gaspar, D.; Pandit, A.; Zeugolis, D. I. The Biophysical, Biochemical, and Biological Toolbox for Tenogenic Phenotype Maintenance in Vitro. *Trends Biotechnol.* **2014**, *32* (9), 474–482. https://doi.org/10.1016/j.tibtech.2014.06.009.

(45) Bax, D. V.; Rodgers, U. R.; Bilek, M. M. M.; Weiss, A. S. Cell Adhesion to Tropoelastin Is Mediated via the C-Terminal GRKRK Motif and Integrin Avβ3. *J. Biol. Chem.* **2009**, *284* (42), 28616–28623. https://doi.org/10.1074/jbc.M109.017525.

(46) Lee, P.; Bax, D. V.; Bilek, M. M. M.; Weiss, A. S. A Novel Cell Adhesion Region in Tropoelastin Mediates Attachment to Integrin Avβ5. *J. Biol. Chem.* **2014**, *289* (3), 1467–1477. https://doi.org/10.1074/jbc.M113.518381.

(47) Madhurakkat Perikamana, S. K.; Lee, J.; Ahmad, T.; Kim, E. M.; Byun, H.; Lee, S.; Shin, H. Harnessing Biochemical and Structural Cues for Tenogenic Differentiation of Adipose Derived Stem Cells (ADSCs) and Development of an in Vitro Tissue Interface Mimicking Tendon-Bone Insertion Graft. *Biomaterials* **2018**, *165*, 79–93. https://doi.org/10.1016/j.biomaterials.2018.02.046.

(48) Nowotny, J.; Aibibu, D.; Farack, J.; Nimtschke, U.; Hild, M.; Gelinsky, M.; Kasten, P.; Cherif, C. Novel Fiber-Based Pure Chitosan Scaffold for Tendon Augmentation: Biomechanical and Cell Biological Evaluation. *J. Biomater. Sci. Polym. Ed.* **2016**, *27*

(10), 917–936. https://doi.org/10.1080/09205063.2016.1155879.

(49) Rodrigues, M. T.; Reis, R. L.; Gomes, M. E. Engineering Tendon and Ligament Tissues: Present Developments towards Successful Clinical Products. *J. Tissue Eng. Regen. Med.* **2013**, *7* (9), 673–686. https://doi.org/10.1002/term.1459.

(50) Engebretson, B.; Mussett, Z. R.; Sikavitsas, V. I. The Effects of Varying Frequency and Duration of Mechanical Stimulation on a Tissue-Engineered Tendon Construct. *Connect. Tissue Res.* **2017**, *8207* (May), 1–11. https://doi.org/10.1080/03008207.2017.1324431.

(51) Gonçalves, A. I.; Gershovich, P. M.; Rodrigues, M. T.; Reis, R. L.; Gomes, M. E. Human Adipose Tissue-Derived Tenomodulin Positive Subpopulation of Stem Cells: A Promising Source of Tendon Progenitor Cells. *J. Tissue Eng. Regen. Med.* **2017**. https://doi.org/10.1002/term.2495.

(52) Islam, A.; Mbimba, T.; Younesi, M.; Akkus, O. Effects of Substrate Stiffness on the Tenoinduction of Human Mesenchymal Stem Cells. *Acta Biomater.* **2017**, *58*, 244–253. https://doi.org/10.1016/j.actbio.2017.05.058.

(53) Liu, C.; Luo, J. W.; Liang, T.; Lin, L. X.; Luo, Z. P.; Zhuang, Y. Q.; Sun, Y. L. Matrix Stiffness Regulates the Differentiation of Tendon-Derived Stem Cells through FAK-ERK1/2 Activation. *Exp. Cell Res.* **2018**, *373* (1–2), 62–70.

https://doi.org/10.1016/j.yexcr.2018.08.023.

(54) Achterberg, V. F.; Buscemi, L.; Diekmann, H.; Smith-Clerc, J.; Schwengler, H.; Meister, J. J.; Wenck, H.; Gallinat, S.; Hinz, B. The Nano-Scale Mechanical Properties of the Extracellular Matrix Regulate Dermal Fibroblast Function. *J. Invest. Dermatol.* **2014**, *134* (7), 1862–1872. https://doi.org/10.1038/jid.2014.90.

(55) Snedeker, J. G.; Foolen, J. Tendon Injury and Repair – A Perspective on the Basic Mechanisms of Tendon Disease and Future Clinical Therapy. *Acta Biomater.* **2017**, *63*, 18–36. https://doi.org/10.1016/j.actbio.2017.08.032.

(56) Gonçalves, A. I.; Rodrigues, M. T.; Lee, S. J.; Atala, A.; Yoo, J. J.; Reis, R. L.; Gomes, M. E. Understanding the Role of Growth Factors in Modulating Stem Cell Tenogenesis. *PLoS One* **2013**, *8* (12), e83734. https://doi.org/10.1371/journal.pone.0083734.

(57) Schneider, M.; Angele, P.; Järvinen, T. A. H.; Docheva, D. Rescue Plan for Achilles: Therapeutics Steering the Fate and Functions of Stem Cells in Tendon Wound Healing. *Adv. Drug Deliv. Rev.* **2017**. https://doi.org/10.1016/j.addr.2017.12.016.

(58) Yeo, G. C.; Baldock, C.; Tuukkanen, A.; Roessle, M.; Dyksterhuis, L. B.; Wise, S. G.; Matthews, J.; Mithieux, S. M.; Weiss, A. S. Tropoelastin Bridge Region Positions the Cell-Interactive C Terminus and Contributes to Elastic Fiber Assembly. *Proc. Natl.*

Acad. Sci. **2012**, *109* (8), 2878–2883. https://doi.org/10.1073/pnas.1111615108.

(59) Yeo, G. C.; Keeley, F. W.; Weiss, A. S. Coacervation of Tropoelastin. *Adv. Colloid Interface Sci.* **2011**, *167* (1–2), 94–103. https://doi.org/10.1016/j.cis.2010.10.003.

(60) Vining, K. H.; Mooney, D. J. Mechanical Forces Direct Stem Cell Behaviour in Development and Regeneration. *Nat. Rev. Mol. Cell Biol.* **2017**, *18* (12), 728–742. https://doi.org/10.1038/nrm.2017.108.

(61) Gonçalves, A. I.; Berdecka, D.; Rodrigues, M. T.; Reis, R. L.; Gomes, M. E. Bioreactors for Tendon Tissue Engineering. In *Bioreactors for Stem Cell Expansion and Differentiation*; CRC Press, 2018; pp 269–300. https://doi.org/10.1201/9780429453144-10.

For Table of Contents Only